J. Magn. Soc. Jpn., 30, 641-645 (2006) <Paper>

An Ultra-Compact Circulator Using Two-Dimensional Magneto-Optical Photonic Crystals

Shanhui Fan and Zheng Wang
Department of Electrical Engineering, Stanford University, Stanford, CA 94305

We present a design of on-chip optical circulator that is ultra-compact, with a footprint on a single-wavelength scale, using rotating non-reciprocal states in a two-dimensional magneto-optical photonic crystal. Both analytic theory and detailed finite difference time domain simulations are presented to illustrate the operating principle of the device.

Key words: circulator; magneto-optical photonic crystals.

1. Introduction

One of the most fundamental challenges to the creation of on-chip, large-scale integrated optics has been to provide signal isolation and to suppress parasitic reflections between devices. In this context, there is a very strong interest in the miniaturization of non-reciprocal optical devices and their on-chip integration[1]. Due to the weakness of magneto-optical effects, conventional devices require a long propagation distance and occupy a large footprint. Thus, it should be very fruitful to explore the enhancement of magneto-optical effects in photonic crystals[2], for the purpose of creating ultra-compact devices with enhanced functionalities.

From a fundamental point of view, the key feature of non-reciprocal photonic crystals is the violation of time-reversal symmetry and reciprocity. As a result, the band structures[3] and the transport properties of photons exhibit characteristics that are completely different from conventional reciprocal systems. Formulating the basic theoretical framework, and developing the mathematical techniques and simulation algorithms for such systems, are therefore of fundamental importance in order to understand this new class of photonic crystal structures.

In this paper we review some of our recent works on both the analytic theory, and detailed numerical design of an ultra-compact optical isolator using cavities in two-dimensional magneto-optical photonic crystals[4),5]. Such a component is important for on-chip optical isolation. Using this example, we also seek to highlight some of the general aspects of modal properties in magneto-optical photonic crystal systems.

2. Modal analysis of magneto-optical resonators

At optical wavelengths, the property of a magneto-optical material is typically characterized by a gyrotropic dielectric tensor $\vec{\varepsilon}$ [6]

$$D = \vec{\varepsilon} E = \varepsilon_0 E + j\varepsilon_a \hat{M} \times E \equiv \left(\varepsilon_0 + \vec{\varepsilon}'\right) E \qquad (1)$$

where ε_0 is the dielectric constant in the absence of magnetization, ε_a measures the strength of the magneto-optical effects, and $\hat{M}$ is the unit vector indicating the direction of magnetization. When the magnetization is along the z direction, the dielectric tensor in (1) assumes the following form:

$$\vec{\varepsilon} = \begin{pmatrix} \varepsilon_0 & \pm i\varepsilon_a & 0 \\ \mp i\varepsilon_a & \varepsilon_0 & 0 \\ 0 & 0 & \varepsilon_0 \end{pmatrix}, \qquad (2)$$

in which the off-diagonal elements has their signs dictated by the direction of magnetization. The strength of magneto-optical effects is measured by the Voigt parameter $Q_M = \varepsilon_a / \varepsilon_0$. For most transparent materials, the Voigt parameter is typically less than 10^{-3} [6].

To theoretically describe modes in a magneto-optical photonic crystal system, we start with the Master equations for photonic crystals[7], where the magnetic field H in the steady state at an angular frequency ω is obtained by solving the eigenvalue equation

$$\Theta|H\rangle = \nabla \times \vec{\varepsilon}^{-1} \nabla \times |H\rangle = \left(\frac{\omega}{c}\right)^2 |H\rangle \qquad (3)$$

In general, this equation can be solved numerically using existing techniques for photonic crystal band structure calculations[8]. To highlight the essential feature of magneto-optical photonic crystals, however, we take advantage of the fact that the Voigt parameter is very weak to develop a perturbation theory. Starting from Eq. (3) and expanding to first order in ε_a, we have

$$\Theta|H\rangle = \nabla \times \frac{1}{\varepsilon_0} \nabla \times |H\rangle - \nabla \times \frac{\vec{\varepsilon}'}{\varepsilon_0^2} \nabla \times |H\rangle = \left(\frac{\omega}{c}\right)^2 |H\rangle \qquad (4)$$

In Eq. (4), $\Theta_0 \equiv \nabla \times \frac{1}{\varepsilon_0} \nabla \times$ describes a photonic crystal in the absence of magneto-optical effects. The effects of magneto-optics can now be treated in terms of the coupling of eigen-modes of Θ_0 as induced by the

perturbation $V \equiv -\nabla \times \frac{\ddot{\varepsilon}'}{\varepsilon_0^2} \nabla \times$.

For two normalized eigenmodes $|H_{1,2}\rangle$ for Θ_0 at eigen-frequencies $\omega_{1,2}$, the coupling constant between them as induced by V can be calculated as:

$$\begin{aligned} V_{12} &\equiv \langle H_1 | V | H_2 \rangle \\ &= -\int H_1^* \cdot \nabla \times \frac{\ddot{\varepsilon}'}{\varepsilon_0^2} \nabla \times H_2 = -\int \left(\nabla \times H_1^*\right) \cdot \frac{\ddot{\varepsilon}'}{\varepsilon_0^2} \left(\nabla \times H_2\right) \\ &= -\omega_1 \omega_2 \int E_1^* \cdot \ddot{\varepsilon}' \cdot E_2 = -\omega_1 \omega_2 \int E_1^* \cdot j\varepsilon_a \hat{M} \times E_2 \\ &= \omega_1 \omega_2 \int j\varepsilon_a \hat{M} \cdot \left(E_1^* \times E_2\right) \end{aligned} \quad (5)$$

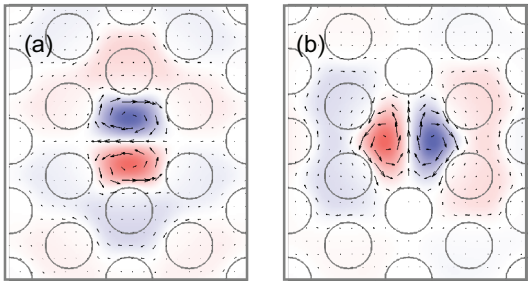

Fig. 1. The thin lines indicate the position of the air holes introduced in a dielectric background of $\varepsilon = 6.25$. The red and blue colors represent large positive and negative magnetic field, which is polarized out of the plane. The vector plots represent the electric fields.

As a concrete example of some of the physical consequences of magneto-optical coupling, we consider a two-dimensional crystal shown in Fig. 1. The structure consists of a triangular lattice of air holes in Bismuth Iron Garnet. The air holes have a radius of 0.35*a*, where *a* is the lattice constant. The corresponding non-magnetic photonic crystal exhibits a large band gap for TE modes that have electric field polarized in the plane[7]. Filling one of the air holes creates a pair of degenerate dipole modes in the photonic band gap. These two modes can be categorized as an even mode $|e\rangle$ (Fig. 1a) and an odd mode $|o\rangle$ (Fig. 1b) with respect to a mirror plane of the crystal.

In the presence of magneto-optical materials, the two modes $|e\rangle$ and $|o\rangle$ couple with each other. The system is now described by a 2×2 matrix:

$$\Theta = \begin{pmatrix} \omega_e^2 & V_{eo} \\ -V_{eo} & \omega_o^2 \end{pmatrix}. \quad (6)$$

Since the two modes are standing waves that possess real-valued electric fields, the coupling constant V_{eo} as described by Eq. (5) is purely imaginary. For this system, which has C_{6v} symmetry, $\omega_e = \omega_o \equiv \omega_0$. With the presence of magneto-optical materials in the cavity, the eigenmodes of the systems, denoted as $|+\rangle$ and $|-\rangle$, now take the form of a rotating wave:

$$|\pm\rangle = |e\rangle \pm i|o\rangle \quad (7)$$

with the frequencies located at

$$\omega_\pm = \omega_0 \pm \frac{|V_{eo}|}{2\omega_0}. \quad (8)$$

The above modal analysis reveals some of the most interesting properties about magneto-optical photonic crystals in general:

(1) Time-reversal symmetry breaking. Since the two counter-rotating modes $|\pm\rangle$ are related by a time-reversal operation, the frequency splitting between them clearly indicates the breaking of time-reversal symmetry and reciprocity.

(2) Fundamental suppression of the effects of disorder by time-reversal symmetry breaking. Even in the case where ω_e deviates from ω_o, for example, due to fabrication related disorder that breaks the three-fold rotational symmetry, as long as the magneto-optical coupling is sufficiently strong, i.e. $|V_{eo}| >> |\omega_e - \omega_o| \omega_e$, $|e\rangle \pm i|o\rangle$ remain the eigenstates of the system. Thus, in the limit of strong magneto-optical coupling, the rotating waveform of the eigen-modes is independent of the slight structural disorders that would almost always occur in practical devices.

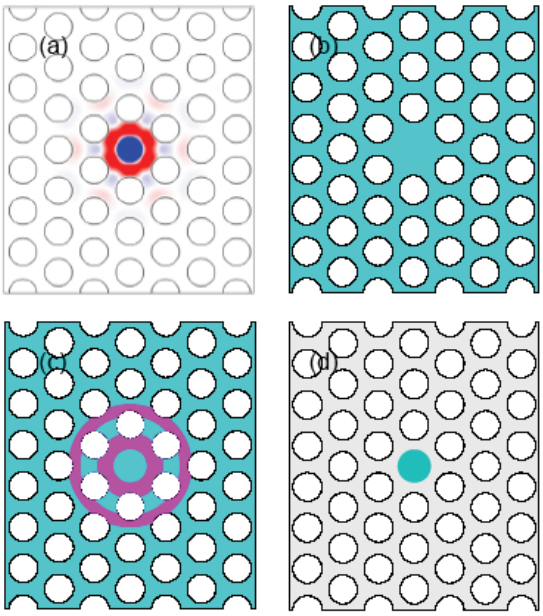

Fig. 2. (a) The out-of-plane component of the cross-product between the electric fields of the two modes shown in Fig. 1. (b) and (c) Green and Purple represent domains with either positive or negative magnetization along the out-of-plane direction. (d) The gray region is non-magnetic. The green region represents a single magnetic domain.

3. Magneto-optical coupling strength

In a magneto-optical photonic crystal cavity, the presence of strength of non-reciprocal effect is directly related to the coupling constant *V*. Examining Eq. (5), we note that the strength of the magneto-optical coupling is strongly influenced by the magnetic domain structures. For the cavity structure as shown in Fig. 1, The cross product $E_e \times E_o$ changes sign rapidly within the cavity (Fig. 2a). Thus, a cavity completely covered by a uniform domain structure (Fig. 2b), in spite of the presence of magneto-optical material, has a very weak magneto-optical coupling strength and essentially behaves as a reciprocal optical resonator. On the other hand, designing the domain structures according to the sign of the modal cross product can maximize the magneto-optical coupling (Fig. 2c). Alternatively, strong coupling can also be achieved with the use of a single domain that covers the center area of the cavity where the modal cross product does not change sign (Fig. 2d). Rewriting the domain structure alone, as can be accomplished by applying external magnetic field or local heating, can thus reconfigure magneto-optical circuits.

Below, we show that these unusual modal properties of magneto-optical photonic crystals lead to remarkable transport properties in ultra-compact, magneto-optical photonic-crystal circuits.

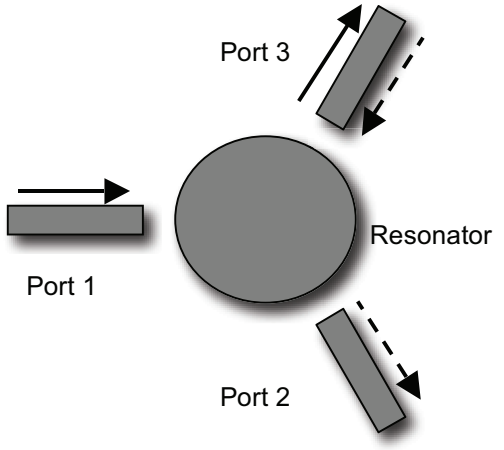

Fig. 3. Schematic of an optical circulator consisting of three waveguides coupled to a resonator.

4. Ultra-compact magneto-optical circulator

As an application of the rotating states in the magneto-optical resonators, as discussed above, we now construct an optical circulator by using these rotating modes to create direction-dependent constructive or destructive interference. The structure is schematically shown in Fig. 3, with three branches of waveguides (ports) evanescently coupled to a resonant cavity at the center. For simplicity, we assume the structure have 120-degree rotational symmetry. Ideally, at the signal frequency the device shall allow complete transmission from ports 1 to 3, 3 to 2, and 2 to 1, while prohibiting transmission in the reversed directions. This transport characteristic can be accomplished with an appropriate choice of frequency splitting between the two counter-rotating states inside the resonator.

The system as shown in Fig. 3 can be described by the following temporal coupled mode theory equations[9)-11)]:

$$\frac{d}{dt}\begin{pmatrix} a_+ \\ a_- \end{pmatrix} = \begin{pmatrix} i\omega_+ - \gamma & 0 \\ 0 & i\omega_- - \gamma \end{pmatrix}\begin{pmatrix} a_+ \\ a_- \end{pmatrix} + \mathbf{K}^T \begin{pmatrix} S_{1+} \\ S_{2+} \\ S_{3+} \end{pmatrix}, \qquad (9)$$

$$\begin{pmatrix} S_{1-} \\ S_{2-} \\ S_{3-} \end{pmatrix} = \begin{pmatrix} -1 & 0 & 0 \\ 0 & -1 & 0 \\ 0 & 0 & -1 \end{pmatrix}\begin{pmatrix} S_{1+} \\ S_{2+} \\ S_{3+} \end{pmatrix} + \mathbf{D}\begin{pmatrix} a_+ \\ a_- \end{pmatrix}. \qquad (10)$$

$a_{+(-)}$ is the normalized field amplitude of the counter-clockwise (clockwise) rotating mode. These modes resonate at frequencies $\omega_{+(-)}$ and decay at rates γ. (Here for simplicity we assume the same decay rate for the two cavity modes.) $S_{i+(-)}$ is the normalized amplitude of the incoming (outgoing) wave at port *i*. The 3x2 matrices, $\mathbf{K}$ and $\mathbf{D}$, represents the coupling between the resonances and the waves at the ports. Unique in magneto-optical system under DC magnetic bias, the full time-reversal operation should include the reversal of external DC magnetic field. Thus, a full time-reversal operation flips the rotation directions of the cavity modes, and hence transform $\mathbf{K}$ to $\mathbf{K}^*$. Taking into account the 3-fold rotational symmetry, and the energy conservation and time-reversal properties of the structure, and following the same procedure as in [10)], we can arrive at the following relations:

$$\mathbf{K}^* = \mathbf{D} = \begin{pmatrix} \sqrt{2\gamma/3} & \sqrt{2\gamma/3} \\ e^{-i2\pi/3}\sqrt{2\gamma/3} & e^{i2\pi/3}\sqrt{2\gamma/3} \\ e^{-i4\pi/3}\sqrt{2\gamma/3} & e^{i4\pi/3}\sqrt{2\gamma/3} \end{pmatrix}. \qquad (11)$$

When wave at frequency ω is incident from port 1, the power transmission coefficients at ports 2 and 3 are solved from Eqs. (8)-(13) as:

$$T_{1\to 2} = \left|\frac{2}{3}\left(\frac{\exp(i4\pi/3)}{1+i(\omega-\omega_+)/\gamma} + \frac{\exp(i2\pi/3)}{1+i(\omega-\omega_-)/\gamma}\right)\right|^2,$$
$$T_{1\to 3} = \left|\frac{2}{3}\left(\frac{\exp(i2\pi/3)}{1+i(\omega-\omega_+)/\gamma} + \frac{\exp(i4\pi/3)}{1+i(\omega-\omega_-)/\gamma}\right)\right|^2, \qquad (12)$$

The ideal circulator response with $T_{1\to 3}=1$ and $T_{1\to 2}=0$ can be obtained at an operational frequency ω_0, when the resonant frequencies are chosen to satisfy the following conditions:

$$\omega_\pm = \omega_0 \pm \gamma/\sqrt{3} \qquad (13)$$

In such a case, ports 2 and 3 function as the output and the isolated ports, respectively. (The roles of ports 2 and 3 are switched with $\omega_+ < \omega_-$.) The bandwidth for 30-dB isolation can be determined to be $0.0548|\omega_+ - \omega_-|/\pi$ in the vicinity of ω_0 using Eq. (14). Also, by rotational symmetry of the structure, we have $T_{1\to2} = T_{2\to3} = T_{3\to1} = 0$, and $T_{2\to1} = T_{3\to2} = T_{1\to3} = 1$. Thus, transmission at frequency ω_0 is allowed only along the clockwise direction. Such a structure therefore behaves as an ideal circulator.

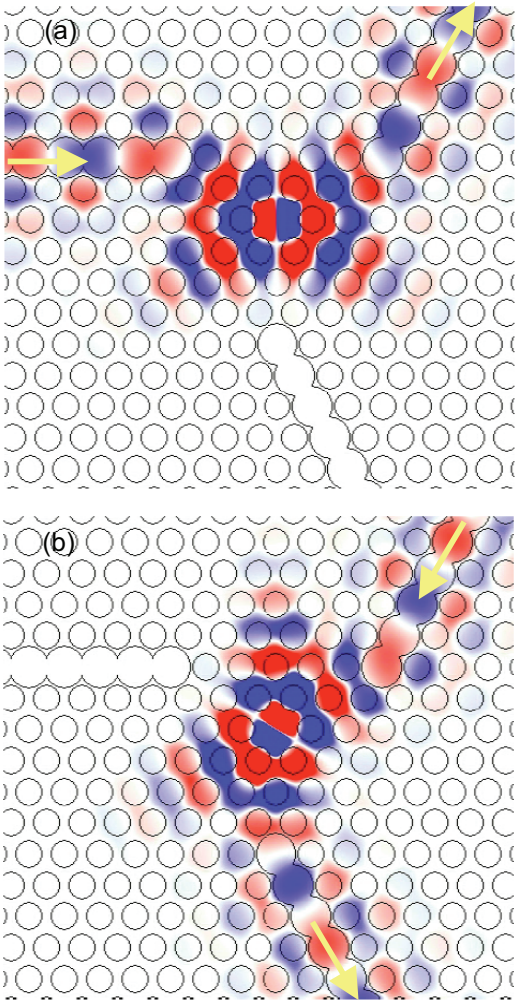

Fig. 4. Steady state field distributions for an optical isolator in a photonic crystal. The thin lines represent the position of the holes. Red and blue refer to large positive or negative magnetic fields. The yellow arrows indicate the direction of propagation.

5. Numerical Simulations

To validate the theoretical analysis, we compare the analytical coupled-mode theory of the previous section with first-principle FDTD calculations with a gyrotropic material model. Each waveguide is constructed by enlarging the radius of a row of air holes to 0.55*a*. (Fig. 4) Such waveguides are single-moded at the mid-gap frequencies. These waveguides are spatially arranged to preserve the three fold rotational symmetry. This configuration also provides excellent control over the coupling between the cavity mode and the waveguides, as the quality factor increases monotonically with distance between the waveguide and the cavity. The cavity has the magnetic domain structure as shown in Fig. 2(c). To reduce computational costs we only include the magneto-optical domain in the vicinity of the cavity region. Filling the remaining computational cell with a single-magnetic domain shows no noticeable differences in the transport properties, since the fields are strongly localized in the cavity region and the waveguides are reciprocal due to the symmetric domain structure. Thin bands of nonmagnetic region have been placed at the air-dielectric interface around the air holes to prevent numerical instability in FDTD simulations. The presence of these bands slightly reduced the maximum magneto-splitting achievable in time-domain calculation for given value of ε_a. (Since the use of a rectangular grid for triangular lattices itself breaks 3-fold rotational symmetry, we have also compensated the numerical dispersion by small modification in the cavity region.)

In the transmission calculation with FDTD method, we choose ε_a=0.02463. With the choice, the two rotating modes have frequencies 0.3465 (*c/a*) and 0.3471 (*c/a*), and quality factors 364 and 367, satisfying the conditions in Eq. (14). The FDTD calculations indeed demonstrate nearly ideal three-port circulator characteristics and agree nicely with the coupled-mode theory (Fig. 5). The numerical simulations thus confirm the validity of temporal coupled mode theory approach in Section 3. The maximum extinction ratio, defined as the power transmission ratio between the output port and the isolated port, reaches 45dB. The extinction is limited by direct tunneling between the waveguides. The bandwidth for 30dB isolation exceeds 6×10^{-5} (*c/a*).

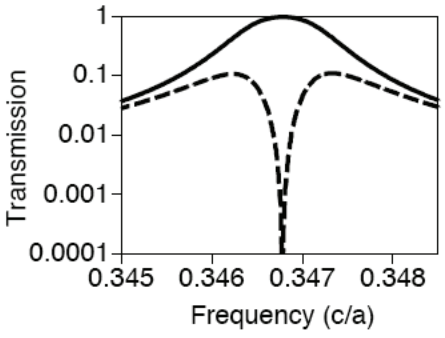

Fig. 5. The solid and dashed lines represent the intensity transmission coefficients to the output and isolated ports, respectively, for the structure shown in Fig. 4.

The steady-state field patterns at a frequency 0.3468(*c/a*), where maximum isolation occurs, are shown in Fig. 4. The magneto-optical resonator shows nearly 100% transmission to the output port and zero transmission to the isolated port (Fig. 4a). Moreover, light incident into the output port is completely dropped to the isolated port (Fig. 4b) and light incident into the isolated port is transferred to the input port. Evidently, an ideal isolator characteristics is observed at the operational frequency and the input port is therefore free from the back reflections from the output port.

6. Concluding remarks

The proposed device occupies only a small footprint of a few wavelength squares. While the simulation in this paper is two-dimensional, the coupled-mode theory analysis, and hence the principles of the device, applies to three-dimensional cavity systems. For implementations in BIG thin films, the material exhibits strong gyrotropy with ε_a saturated at 0.06.[12)-13)] From the coupled-mode theory, the bandwidth of the circulator scales linearly with the magneto-optical coupling strength. Hence the BIG device can provide a large bandwidth for 30dB isolation up to 213GHz, when operating at 633nm. Since the quality factor of the resonator due to waveguide coupling can be as low as 140, the relative large material absorption in BIG can be still tolerated. At optical communication wavelength of 1550nm, Ce:Yttrium Iron Garnet (Ce:YIG) has ε_a saturated at 0.009 with very low absorption[14)]. For this material system, the bandwidth for 30dB isolation at 1550nm is estimated as 12.6GHz.

A hybrid magneto-optical cavity in silicon/air photonic crystal also exhibits large magneto-coupling, while holding the advantage of better compatibility with existing planar integrated optical circuits[4)]. Also, by inverting the magnetization, complete transmission is switched from the output port to the isolated port. (This can be seen in Eq. (5), where inverting the magnetization results in the switch between ω_+ and ω_-.) Therefore, high-density non-volatile reprogrammable optical circuits may be implemented on existing silicon-based technology.

Acknowledgements. This work is supported in part by a David and Lucile Packard Fellowship in Science and Engineering.

References

1) M. Levy, IEEE J. Sel. Top. Quantum Electron. 8, 1300 (2002).
2) M. Inoue, K. Arai, T. Fujii, and M. Abe, *J. Appl. Phys.*, 85, 5768 (1999).
3) A. Figotin and I. Vitebsky, *Phys. Rev. E*, 63, 066609 (2001).
4) Z. Wang and S. Fan, *Appl. Phys. B*, 81, 369 (2005).
5) Z. Wang and S. Fan, *Opt. Letts.*, 30, 1989 (2005).
6) A. K. Zvezdin, V. A. Kotov, *Modern Magnetooptics and Magnetooptical Materials*. (Institute of Physics Publishers, Bristol, 1997).
7) J. D. Joannopoulos, R. D. Meade, and J. N. Winn, *Photonic Crystals: Molding the Flow of Light*. (Princeton University Press, Princeton, NJ, 1995).
8) S. G. Johnson and J. D. Joannopoulos, *Opt. Express*, 8, 173 (2001).
9) H. A. Haus, *Waves and fields in optoelectronics*, (Prentice-Hall, Englewood Cliffs, NJ, 1984).
10) S. Fan, W. Suh, and J. D. Joannopoulos, *J. Opt. Soc. Am. A*, 20, 569 (2003).
11) W. Suh, Z. Wang, and S. Fan, *IEEE J. Quantum Electron.*, 40, 1511 (2004).
12) T. Tepper and C. A. Ross, *J. Cryst. Growth*, **255**, 324 (2003).
13) N. Adachi, V. P. Denysenkov, S. I. Khartsev, A. M. Grishin, and T. Okuda, *J. Appl. Phys.* **88**, 2734 (2000).
14) M. Huang and S. Y. Zhang, *Appl. Phys. A*, **74**, 177 (2002).

Received Jun. 14, 2006; Accepted Aug. 21, 2006.